RSC Advances

ROYAL SOCIETY OF CHEMISTRY

www.rsc.org/advances

Cite this: DOI: 10.1039/c0xx00000x

www.rsc.org/xxxxxx

ARTICLE TYPE

Visible-light photocatalysis on C-doped ZnO derived from polymer-assisted pyrolysis

Ahmad S. Alshammari,[a]* Lina Chi, [b,c] Xiaoping Chen,[b,c] Abdulaziz Bagabas,[a] Nazanin Rashidi-Alavijeh,[d] Denis Kramer,[b]Abdulaziz Alromaeh,[a]Zheng Jiang[b]*

Received (in XXX, XXX) XthXXXXXXXXX 20XX, Accepted Xth XXXXXXXXX 20XX
DOI: 10.1039/b000000x

C-doped ZnO with large surface area was prepared via F127-assisted pyrolysis at 500 °C and used for visible-light-responsive photocatalytic water purification. The bandstructure of the C-doped ZnO was investigated using valance band XPS and DFT simulation. The C-doped ZnO possessed enhanced absorption to UV and visible light, though it showed lower visible-light-responsive photocatalytic activity than ZnO because of significant recombination of photogenerated charge carriers arisen from overloaded C-dopant and oxygen vacancies.

1.Introduction

Solar energy photocatalysis on heterogeneous photocatalystsis a promising sustainableprocess for environment remediation and artificial photosynthesis, while its viability in practice highly depends on the effective photocatalysts[1-4]. Among variousphotocatalysts, ZnO and TiO_2 are most plausible due to their high photosensitivity, nontoxicity, low cost though they can only utilise a small portion of solar energy (3-5%) in UV regionowing to their large bandgap[5-8]. Similar to TiO_2, ZnO possesses great potential in modulation of bandgap for harvesting visible light but it is easier to crystalise and manufacturedevices[5, 9, 10]. The bandgap of ZnO may be tuned via doping with non-metal or transition metal, or hybridising with other small-bandgap semiconductor or metal to form Shockley junctions, or creating structural vacancies[1, 5, 11, 12]. Motivated by the success to enhance visible-light response of non-metal-doped TiO_2, non-metal-doped ZnOhave been extensively attempted because the non-metal (S, N or C) dopants can extend visible light absorption significantly and well suppress photogenerated charge recombination at su`itable doping level[7, 9, 13-19].

C-doped ZnOis an emerging visible-light-responsive photocatalyst with desirable performance in cleaning up waste water, water splitting and photoelectrochemical cells[7-9, 11, 20]. Although synthesis of C-doped ZnO represents a considerable challenge, a few methodologies have been successfully established, includingself-doping via thermal decomposition of $Zn_5(CO_3)_2(OH)_6$ precursor[7], pyrolysis of Zn-containing inorganic-organic presursors,[8, 14]polymer or carbon templatedsyntheses[9], metal organic chemical vapour deposition (MOCVD)[21] and thermal plasma in-flight carbonisation techniques[22].The polymer-assisted pyrolysis synthesis allows incorporation carbon into ZnOmatrix and improving its porosity[8, 14].However, differentC-doping species ormulti-level oxygen vacancies (Ovac)would co-existed in the resultantC-doped ZnO materials[7, 23], resulting in the difficulty to clarify the origin of visible-light response of C-doped ZnO, so did C-doped TiO_2[16, 18, 19].In principle, light C-doping may extend visible-light absorption and promote their visible-light-driven photocatalysis[8, 12, 23, 24], while heavy C-doping is highly possible to result in recombination ofphotogenerated charge carriers. Therefore, it is essential to investigate the roles of C-dopant and Ovacin the harvesting visible-light and visible-light-responsive photocatalysisforC-doped ZnO with heavy C-doping level.

In this study, Pluronic F127 ($EO_{106}PO_{70}EO_{106}$) copolymer was adopted for incorporating carbon into ZnO and improves its porosity through a polymer-assisted thermal pyrolysis at 500 °C. The crystal phase, morphology, porosity, light absorption properties and carbon species of the received C-doped ZnO were carefully characterised. The origin of the visible-light response of the C-doped ZnO was interpreted via valance band XPS and first-principle simulation using CASTEP pakage. The photocatalysis performance of ZnO and C-doped ZnO was comparatively evaluated under visible-light to conclude the roles of C-doping.

2.Experimental and computational

2.1 Sample preparation

All the chemicals were of reagent-grade and were used as purchased from Sigma-Aldrich Company without further purification. Deionized water was used in all experiments.

In the synthesis of C-doped ZnO, 5.9 g of $Zn(NO_3)_2{\cdot}6H_2O$ was dissolved in 50 ml of mixed solution of deionized water and ethanol (water:ethanol=1:1 in volume ratio) to form a clear solution, then 0.75 g of F127 was added. The resulting mixed solution wasmoved into an electric oven at 90 °C andheated overnight to vapour solvents and form dry polymer metal-organic complex. The dry complex was calcined in muffle furnace up to 500 °C for 3 hours in a 2 °C/min heating ramp. For comparison, a pristine ZnO was also prepared in the same procedure without addition of F127.

2.2 Characterisation

X-Ray diffraction (XRD) patterns were obtained on a Philip X'Pert D using Cu-Kα1 radiation at a scan rate of 0.05° 2θ/s and were used to determine the phase structures of the samples. Transmission electron microscopy (TEM) analysis was conducted using a JEM-2100F microscope (JEOL, Japan) at a 200 kV accelerating voltage. Photocatalyst samples were dispersed in water/methanol and treated with ultrasound for 5 min before deposited on a carbon coated grid.

Brunauer, Emmett, and Teller (BET) surface areas and pore size distribution of the photocatalysts were obtained on Micrometrics Gemini III-2375 (Norcross, GA, USA) instrument by N_2physisorption at -196 °C. Prior to the measurements, the catalyst was evacuated for 2 h at 150 °C to remove physically adsorbed water. The BET surface area was determined by a multipoint BET method using the adsorption data in the relative pressure (P/P_0) range of 0.05-0.3.

The UV–vis diffuse reflectance spectra were obtained on Perkin Elmer Lambda 950 UV/Vis/NIR spectrophotometer equipped with a 150 mm snap-in integrating sphere for capturing diffuse and specular reflectance. $BaSO_4$ was used as a reflectance standard in the UV-visible diffuse reflectance experiment.

X-Ray photoelectron spectroscopy (XPS) measurements were performed on the ESCALAB-210 spectrometer (Thermo VG Scientific, UK) with an Mg-Kα source. All the binding energies were referenced to the C 1s peak at 284.6 eV of the surface adventitious carbon.

2.3 Photocatalytic activity

The photocatalytic activity of the prepared samples in terms of the photocatalyticdecolorization of methylene blue (MB) aqueous solution was performed at ambient temperature under visible-light irradiation using a 300 W Xe lamp (15 cm above the dishes) with a 400 nm cutoff filter as a light source.

In the photocatalysis experiments, 0.1 g of the prepared photocatalyst powder was dispersed in a 100 mL MB aqueous solution with a concentration of 10 ppm in a beaker. The mixed solution was remained in dark for an hour to establish an MB solution adsorption-desorption equilibrium on the photocatalyst before light irradiation. During photocatalysis, the 4 mL reaction solution was taken out in every 15min irradiation interval and filtered to measure the concentration change of MB using a UV-visiblespectrophotometer (Scinco, Neosys-2000, South Korea). Since the MB was at rather low concentrationin the aqueous solution, its photodegradation followed a pseudo-first-order reaction and its kinetics can be expressed as $-\ln(c/c_0) = kt$,where k is the apparent rate constant and c_0 and c are the initial and reaction concentrations of aqueous MB solution, respectively.

2.4 Computational details

The density function theory (DFT) calculations of ZnO and C-doped ZnO were performed withthe CASTEP package using the generalized gradient approximation (GGA)[25], in the scheme of Perdew-Burke-Ernzerhof (PBE) to describe the exchange-correlation functional. The norm-conserving pseudopotential was adopted rather than ultrasoft pseudopotential because the former is more suitable to simulate the bandgap and optical properties.

For simulating C-doping effects, we first built a 2 × 2 × 2 (32-atom) wurtzite ZnO supercell, containing 16 Zn and 16 O, in which oneO atom was replaced by a C atom, corresponding to C dopinglevel of 6.25 at.%. The crystal parameters of wurtziteZnO unit cellin the DFT calculation are a = 3.249 Å and c = 5.205 Å. The Monkhorst-Packgrid for SCF calculation is 7 × 7 ×4with 16 k points was used for integration in the Brillouin zone of the supercell[26], and the plane-wave kinetic energy cutoff was set to 600 eV. The mechanical equilibrium was achieved through conjugate gradient minimization of the total energy to a tolerance of 2×10^{-6} eV/atom, the maximum forces to a tolerance of 0.05 eV $Å^{-1}$, and the maximum atomic displacement position tolerance of 1×10^{-3} Å. The 2 × 2 × 2 (32-atom) wurtziteZnOsupercell was also simulated as reference.

3. Results and Discussion

3.1 Crystal and textural properties

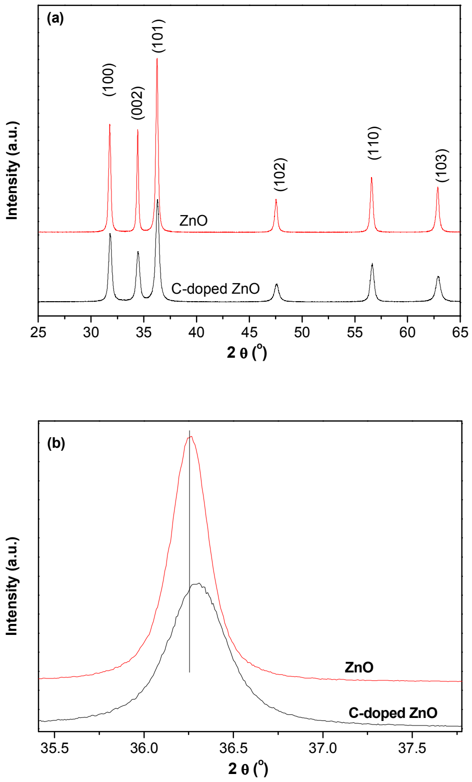

Fig.1 (a) full and (b) amplified XRD patterns of the pristine ZnO and C-doped ZnOcalcined at 500 °C

Fig.1(a) comparatively shows the XRD patterns of pure and C-doped ZnO samples calcined at 500 °C. All the Bragg diffraction peaks of the ZnO and C-doped ZnO samples can be well indexed according to hexagonal wurtziteZnO ($P6_3mc$, JCPDS: 890511), though the C-doped ZnO shows weaker diffraction intensity thanZnO, indicating that C-doped ZnO possesseslower crystallinity or smaller crystallite size. The close observation to the strongest peaks (Fig. 1b) shows the C-doping leads to (101) diffraction shifting to higher 2θ angle, which is ascribed to doping-induced unit cell deformation. As listed in Table 1, the calculated crystallite size, lattice parameters and unit cell volume of C-doped ZnO are indeed smaller than those of pure ZnO. The

C-doping induced ZnOlattice parameters reduction and cell volume shrinking can be reasonably attributed to structure defects (Ovac) caused by C-doping.If there were no Ovac, the lattice parameters should have been increasedbecause the carbon anion radius (69-76 pm) is greater than oxygen (57-66pm). From the charge equilibrium point of view, substitution of O(-II) by C(-IV) would unbalance system charge that requires oxygen loss to remain system neutral. The results agree with previous research where C-doping induced unit cell changes were also observed[22].

Table 1 Structural and textural properties of ZnO and C-doped ZnOcalcined at 500 °C

Sample	Crystallite size (nm)	Lattice parameters(Å)		Unit cell volume (Å^3)	S_{BET} (m^2/g)
		a=b	c		
ZnO	27.2	3.2490	5.2061	47.5936	7.1
C-doped ZnO	21.8	3.2448	5.2015	47.4275	17.1

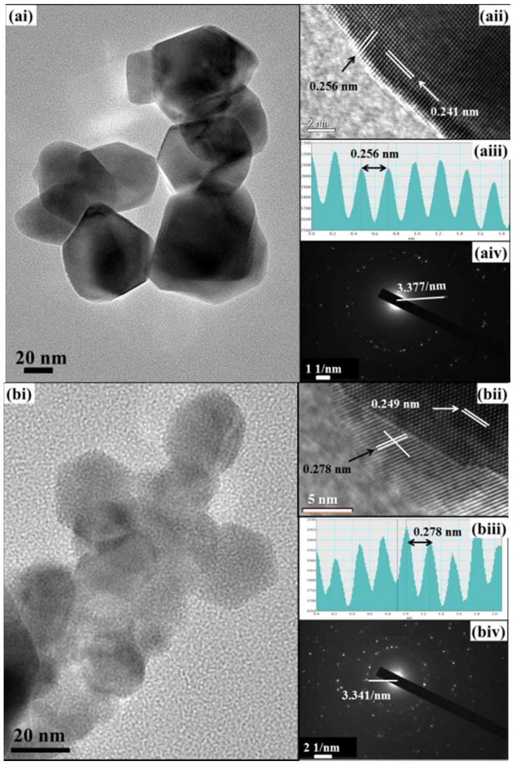

Fig.2. TEM (ai, bi), HRTEM (aii,bii), lattice fringes (aiii, biii) and SAED (aiv, biv) images of (a) ZnO and (b) C-doped ZnOcalcined at 500 °C

Transmission electron microscope (TEM) was used to further investigate the morphology and crystal structures of ZnO and C-doped ZnO. It can be seen from the TEM images (Fig.2) that ZnO and C-doped ZnO are in nano-flake morphology (Fig2 ai and bi), butC-doped ZnOnanoflakes show more regular hexagonal shape and smaller particle size (~20 nm) than that of pure ZnO (~30 nm) , which iswell consistent with XRD results. The HRTEM imagesof ZnO and C-doped ZnO are presented in Fig2 (aii) and (bii), in which the labelled lattice fringes (Fig.2 aiii and Biii) are corresponding to d-spacings between adjacent (100) and (101) surfaces, respectively. The angles between the labelled d-spacings are around 45°, corresponding to the dihedral angle between (100) and (101) surfaces. The HRTEM results reveal the largely exposed plane is (001) surface, which is further evidenced by the selected area electron diffraction patterns (SAED, Fig.2 aiv and biv). The circular multi-spots in the SAED images indicate the samples are polycrystals with (001) surfaceexposedpreferentially.

Polymer surfactants have often used to control morphology and texture of ZnO crystals[27, 28]. Large S_{BET} of 12.5 m^2/g was ever observed on hierarchical C-doped ZnO prepared via a PEG-2000 directed thermal decomposition of $Zn_5(CO_3)_2(OH)_6$ at 500 °C[7], where the high porosity was attributed to ZnOinterparticle slits and intra-flakevoids created by release of volatile gases like CO and H_2O during thermal treatments. However, there were no nano-pores or voids observed on our C-doped ZnO flakes (Fig.2), which is reasonable since ZnO is easy to crystallise before forming regular poresaround the polymer template. In our work, polymer surfactant F127 served as both carbon source and pore direct-agent to form ZnOnanoflakes in the C-doped ZnOpreparation. The specific surface area (S_{BET}) of the C-doped ZnO is 17.1 m^2/g after calcinations at 500 °C (Table 1), approximately 2.5 times that ZnO, and is larger than the hierarchical C-doped ZnO prepared via self-doping strategy[7]. The larger S_{BET} of C-doped ZnOis associated with its smaller particle.

3.2 Optical properties

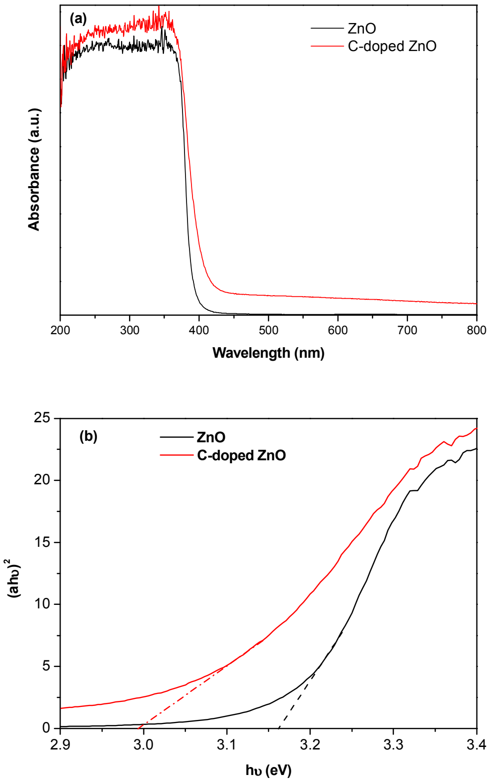

Fig.3 UV-vis diffuse adsorption spectra (a) and corresponding (ahv)^2*v*shv plots for (b) ZnO and C-doped ZnOcalcined at 500 °C

UV-vis diffuse adsorption spectra (UV-DRS) shown in Fig.3 (a)comparatively presents the different light absorption characteristics of pure and C-doped ZnO materials. In comparison with ZnO, C-doped ZnOdisplays significant red shift of optical bandgap absorption edge into visible-light region as well as enhanced light absorption in the whole UV-visible band. Non-metal doping into wideband metal-oxide photocatalysts,such as N-doped TiO_2,may effectively improve their visible-light absorption but cost a price of reduced UV absorption[15, 29]. Although visible-light absorption is important for C-doped ZnO as a photocatalyst,enhanced UV absorbance wouldalsobenefitphotocatalysis application of sunlight since UV is more efficient[14, 16]. Improvement of UV adsorption of C-doped ZnO is highly dependent on the synthesis strategy and precursors. For instance, enhanced UV adsorption was ever observed on C-doped ZnOphotocatalyst derived from zinc gluconate precursor[14], but C-doped ZnO synthesised viaVitamine C or self-doping strategies did not show improved adsorption of UV light[7, 8].

Applying Kubelka-Munk rule the direct bandgap energies of ZnO (3.17 eV) and C-doped (2.98eV)ZnO may be extracted precisely from their $(ahv)^2$*vs*hv plots as shown in Fig.3 (b).More importantly, the $(ahv)^2$*vs*hvplot in bandgap region for C-doped ZnOis linear alike that of ZnO, revealing the C-doping did not change direct electron transition characteristic of ZnO in badgap[7]. Enhanced light harvesting and direct transition characteristics are highly desirable for doped ZnO materials in photocatalysis, opticoelectronicand solar cell applications.

Alike ZnO, the disrupt drop of light-absorption in bandgap regionof C-doped ZnO is observed clearly, suggesting that carbon was incorporated into ZnO matrix rather than laid down on ZnO surface. The C in ZnO lattice would revise ZnO'sbandstructure to introduce impurity midgap(s) and thus tune its bandgap. Besides bandgap light absorption, visible-light absorption on the C-doped ZnOis also tailed beyond 800 nm which is a typical red shift induced by impurity adsorption or oxygen-vacancies (Ovac)[15, 23]. Advanced characterisations are necessary to determine C-species and Ovacfor understanding the nature ofvisible-light response onthe C-doped ZnO.

3.3 Surface component and electron structure

3.3.1XPS analysis

XPS measurements were conducted to analyse surface species and valence band of both ZnO and C-doped ZnO so as to understand the origin of visible-light response of C-doped ZnO. Fig.4 (a)-(d) present the acquired C1s,O1s and Zn 2p core level as well as the valence-band XPS spectra of pure and C-doped ZnOcalcined at 500 °C, which clearly distinguished the differences between ZnO and C-doped ZnOin both core level and valance electron bands.

As shown in Fig.4 (a), two sets of peaks are observed in the C1s XPS spectrafor both pure and C-doped ZnO samples, including a large peak with binding energy (BE) ranging from 282 to 286.5 eV and a satellite peaks at higher BE region. With the same BE centring at 288.7 eV, the satellite peaks for pure and C-doped ZnO samples are attributed to the adsorbed CO_2 and structural carbonate species containing C=O[7, 13]. Such species containing C=O was ever predicted by DFT calculation and evidenced experimentally for C-anion-doped TiO_2[18, 19], whereas the C1s satellite peak is broader, revealing a portion of such C species would be from carbonate species trapped in C-doped ZnO matrix or existing incompletely decomposed carbonate precursors[7].

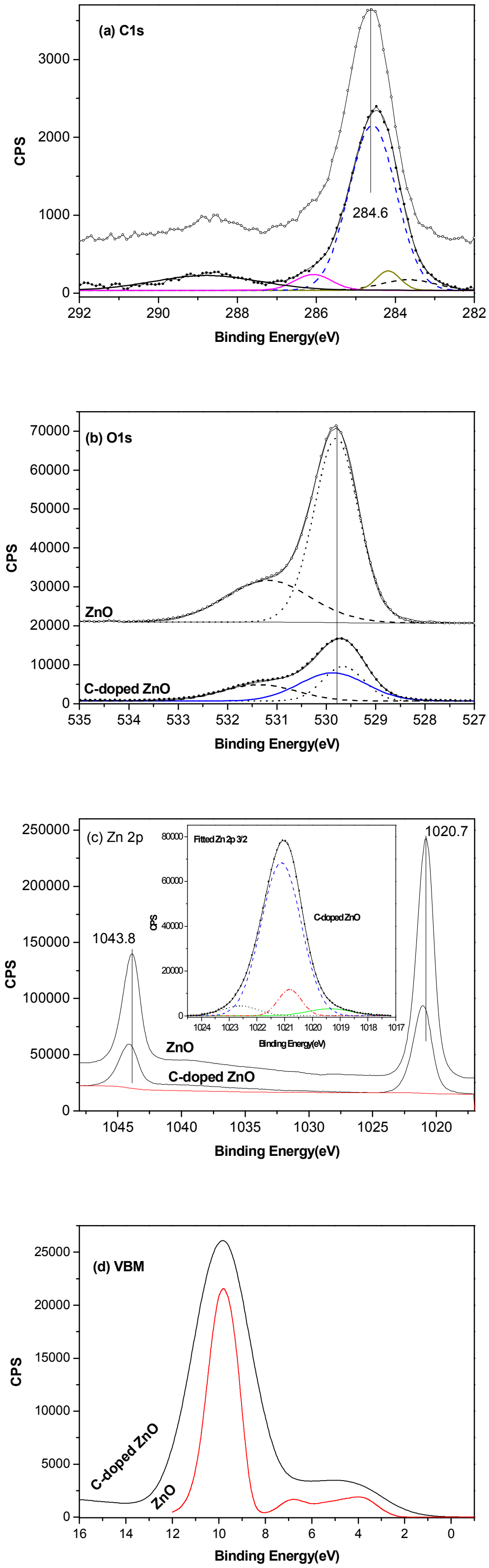

Fig.4 Core level XPS spectra of (a) C1s, (b) O1s, (c) Zn 2p and (d) valence band inZnO and C-doped ZnOphotocatalystscalcined at 500 °C

The major C1s XPS peak of C-doped ZnO is asymmetric and distinct from that of ZnO. The main peak centres at 284.6 eV for

ZnO is symmetric and can be ascribed to adventitious hydrocarbon. However, the asymmetric major peak of C 1s XPS for C-doped ZnOcentres at 284.4 eV, 0.2 eV red-shift relative to that in ZnO, which is resulting from peaks overlap between contaminant carbon and other carbon species. The major C1s XPS peak was therefore fitted into 4 peaks: the largest one at 284.6 eV can be assigned to adventitious hydrocarbon, while 286.2 eV and 283.8 eV are due to Zn-O-C and Zn-C bonds[22], respectively. The smallest fitted peak at 282.9 eV is associated to Zn-C bond connected with oxygen-vacancy (Ovac) since additional electron density would be imposed from negative-charged Ovac onto C in the Zn-C-Ovac bond. It has been well accepted that Ovac may result in bandgap narrowing[23], therefore it is necessary to address the contributions of Zn-C and Ovac to the visible-light response of C-doped ZnO.

The areas of C1s XPS peaks due to Zn-O-C, Zn-C and Zn-C-Ovac are almost the same. In principle, zinc carbonate species would not cause visible light response in ZnO[7], hence, it can be concluded the visible-light-response should be associated directly with Zn-C-Ospecies and Zn-C-Ovac induced by carbon-doping. As discussed in UV-vis-DRS, Ovacwouldmainly be responsible for the light response in the whole visible-light range that accounts for grey colour of our C-doped ZnO, but also influences bandgap adsorption as discussed in electronic structure section.

Fig.4 (b) presents the O1s XPS of pure and C-doped ZnOcalcined at 500 °C. For pure ZnO, a large O 1s locates at 529.8 eV is due to Zn-O bonds in wurtziteZnO crystal, and a shoulder peak (531.3 eV) of 25%height to the major peak may be due to surface chemical adsorbed oxygen species, such as OH^- group and carbonates[22]. The O1s XPS of C-doped ZnO encompasses a major peak at 529.7 eV along with a shoulder peak (531.5 eV) of 33% intensitytothe major peak, suggesting the O1s components locates in differentenvironment from those in ZnO. O1s XPS of C-doped ZnO werefitted into 3 peaks centring at 531.5, 529.9 and 529.7 eV. The peak at 531.5 eV may be ascribed to surface adsorbed oxygen species (OH group) and carbonate species (ie. C-O and C=O bonds). The peak at 529.6 eV is assigned to O^{2-} ions of Zn-O bonds in Wurtzite structure with Zn^{2+}in hexagonal coordinations,andO1s peak at 529.9 eV can be reasonably attributed to Zn-Ovac and Zn-O-C bonds because C-dopant and Ovac usually induce blue shift of Zn-O bond[23]. It is difficult to determine the concentrations of Ovac and Zn-C-O or Zn-O-C species from O1s XPS because thepeaks are heavily overlapped.

Fig. 4(c) compares the Zn 2p XPS spectra of ZnO and C-doped ZnO. It can be clearly seen that the Zn $2p_{3/2}$ and $2p_{5/2}$XPS lines in C-doped ZnO are blue shifted (0.2 eV) systematically relative to pure ZnO. The BE difference between Zn $2p_{3/2}$ and $2p_{5/2}$XPS lines remains 23.1 eV for ZnO and C-doped ZnO, suggesting Zn is in Zn^{2+} state for the two samples[22]. The Zn $2p_{3/2}$ state was further fitted into 4 peaks (inserted in Fig.4 c) corresponding to Zn-C (1019.3, 4.3%), Zn-O-C(1020.8 eV, 8.2%), Zn-O (1021.1 eV, 82.6%) and Zn-O_{vac} (1022.6 eV, 4.9%) bonds, respectively. The results reveal the carbon concentration is around 12.5 atm% relative to Zn, 2.5 times that Ovac concentration. However, the concentration of Zn-C carbide species is nearlyequal to that of Ovac, suggesting the formation of each Zn-C bond would create at least one Ovac site which agrees with the C1s XPS analysis.

Valence band (VB) XPS is a powerful tool to investigate the influence of impurity on the bandstructure of semiconductors. Fig.4 (d) comparatively shows VB XPS spectra acquired on ZnO and C-doped ZnO. It clearly shows the C-doping not only red-shifts valance band maximum (VBM) energy but also expands the VB band width. The VBM of ZnO is approximately 2.24 eV relative to vacuum level yet lifts up to 1.33 eV once doped with carbon, revealing C-doping in this case is an n-type doping. In addition, the ZnO VB with width about 6.0 eV is more localised with clear discrete energy levels than the VB of C-doped ZnO. The VB width of C-doped ZnO is greater than 7.0 eV and overlapped with deeper energy level, revealing its VB electrons are delocalised and more dispersive.

3.3.2 Electronic structure

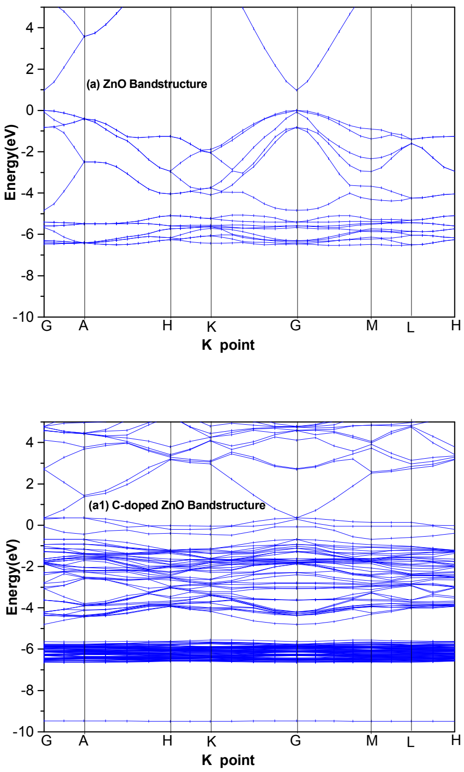

Fig.5 Simulated bandstructures of Wurtzite (a) ZnO and (b) C-doped ZnO

CASTEP code was used to simulate the electron structures of wurtzite ZnO and C-doped ZnO crystals. Fig.5 (a) and (b) compares the simulated bandstructures of ZnO and C-doped ZnO, showing C-doped ZnO possesses much higher electron density of state (DOS) because of C-doping induced electron delocalisation. A new electron density of sate at ~10 eV due to C 2s state is also observed in the C-doped ZnO. The calculated Eg of ZnO is 0.97 eV, which is much smaller than experimental value (3.17 eV) due to the choice of GGA exchange-correlation energy in DFT simulation. However, it is fairly larger than Eg calculated using ultrasoft pseudopotential[7], indicating the advantage of norm-conserving pseudopotential over ultrasoft pseudopotential in bandstructure simulation. simulation using GGA+U function may predict Eg closer to experimental value while it is rather expensive since it estimates Eg based on GGA geometry optimisation[17, 18]. Within our approximation, GGA modelling provided here sufficient accuracy for the influence of C-dopant on the VB position and C donor states relative to the VBM.

The calculated VB width is approximately 5.5 and 6.1 eV for ZnO and C-doped ZnO, respectively, which are well consistent with the VB XPS results. In addition, the conductance band minimum (CBM) was dropped down around 1.0 eV compared to ZnO. The valance band maximum (VBM) and conductance band minimum (CBM) of the pure and C-doped ZnO are both locating at G points, indicating their direct electron transition in bandgap region that are convinced by the experimental UV-vis-DRS characterisation results (Fig.3 b). The VBM of C-doped ZnO joints with its CBM at G point leading to vanishing of bandgap of C-doped ZnO, which is mainly due to a new additional C 2p state on top of O 2p state of ZnO (Fig.7c and Fig.S1 a) as well as the underestimated Eg .

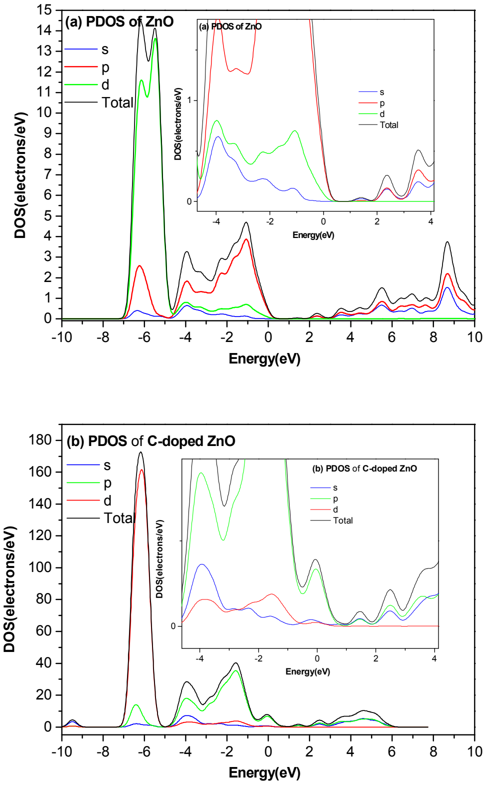

Fig.6 PDOS of Wurtzite structured (a)ZnO and (b) C-doped ZnO crystals

The enhanced DOS, narrowed bandgap and extended bandwidth of C-doped ZnO relative to ZnO are further detailed by the PDOS plots shown in Fig.6 (a) and (b). It can be seen the VB of ZnO is mainly composed of p state electrons well dispersed in the whole VB region as well as s and d states appearing at slightly deeper VB band. The major component of ZnO valance band maximum (VBM) is p state and small amount of d state electrons. The conductance band minimum (CBM) of ZnO is only containing s state electrons. In contrast, the VB of C-doped ZnO is mainly composed of p state electrons but the s and d state electrons also contributed significantly to its VBM. It is notable that the CBM of C-doped ZnO contains s and p state electrons.

Combined Fig. 6 and the element PDOS results presented in Fig.7 (a-c) and Fig.S1(a,b), it can be concluded that the VB of ZnO is composed of hybridised O 2p and Zn 3d states, and its CB comprises of Zn 4s states and O 2p at higher energy level.From the Zn and O PDOS plots in Fig.S1, it may be found ZnO VBM is mainly composed of O2p sates hybridising with a little Zn 3d state, while Zn 4s state dominates the CBM. Once C is incorporated into ZnO, new electron states areappeared at VBM and pinned at Fermi level. The VBM are dominated with C 2p state (Fig.7c) with hybridised Zn 3d and 4s states (Fig.7 a, b and insets). The CBM of C-doped ZnO is dominated by s state with almost equal amount of p state. Apparently, the VBM and CBM components of C-doped ZnO distinctly distinguish from those of ZnO and its reduced bandgap is mainly due to new states arisen from C-doping. The components of CBM in C-doped ZnO are also changed correspondingly in comparison to ZnO.

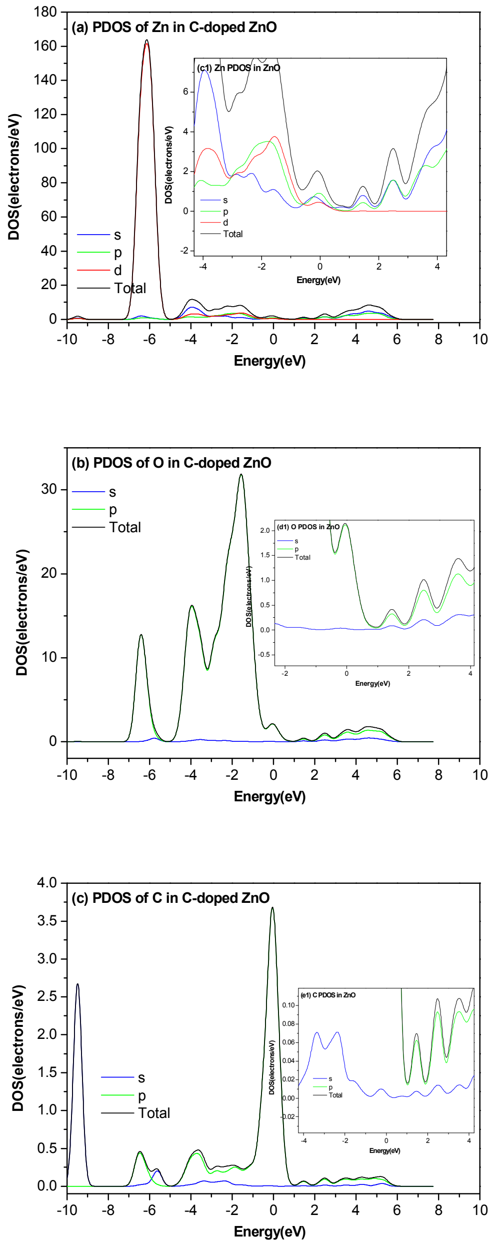

Fig.7 PDOS of Zn(a), O (b) and C (c) of C-doped ZnOWurtzite crystal. Insets correspond to amplified PDOS around bandgap region

It is essential to further investigate the components of the new additional states on top of VBM and CBM which disclose the roles of C-doping in narrowing bandgap of C-doped ZnO. As shown in Fig. 7 (a-c), the detailed PDOS of Zn, O and C in C-doped ZnO verify its VBM state are mainly composed of C 2p sate (~50%), O 2p (~25%) and hybridised 4s and 3d states (25%) of Zn. The new O and Zn states at VBM can be attributed to oxygen vacancies induced by C-doping so as to remain the overall charge neutrality after substitutionof O^{2-} by C^{4-} in ZnO matrix[18]. Although Zn 4s state dominates CBM of C-doped ZnO, O 2p and 2s states also contribute around 25% CBM yet the contribution of C-dopant (2p state) to the CBM is negligible.

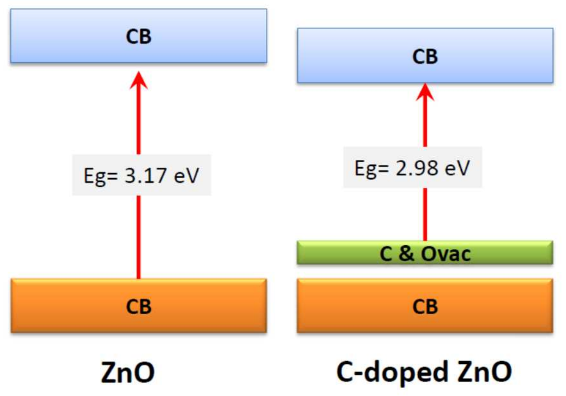

Fig.8 Schematic bandstructures of ZnO and C-doped ZnO crystals

Combining the experimental VBM XPS and theoretical PDOS analyses we can now draw an elusive scheme of band structure of C-doped ZnO as shown in Fig.8, which clearly shows the bandgap narrowing of C-doped ZnOis mainly induced by C-doping and derived Ovac: the new states of C 2p and Ovac-related O 2p, Zn 3d and 4s that lift up VBM of ZnO; Zn 4s and O 2p states related to Ovac comprise of the CBM in C-doped ZnO which pushes the CBM down to lower energy level. In all, it is the additional energy levels induced by C-doping and Ovac narrowing the bandgap of C-doped ZnO in comparison to ZnO.

3.4 Photocatalytic activity

Fig.9 (a) shows the time-dependent absorbance spectra of MB on C-doped ZnO under visible light illumination, reveals the gradual decolourisation of MB on C-doped ZnO under visible light irradiation. The photodegradation should be induced by the photocatalytic reaction because MB degradation is negligible without photocatalyst and no degradation was observed on the photocatalysts in dark. Despite the fact that C-doped ZnO possessed enhanced light absorption, ZnO exhibited notably higher photoactivity in MB degradation than C-doped ZnO under visible light irradiation (Fig.9b). It is well known that photocatalysis follows the first order kinetics law, so that the apparent reaction kinetics constant, k, can be extract from the slope of plot of $-\ln(c/c_0)$ *vs* reaction time[7, 14, 15]. The calculated k values for ZnO and C-doped ZnO are 0.009 and 0.006 min^{-1}, respectively. ZnO possesses better activity and larger k_{ZnO} than C-doped ZnO, suggesting the visible-light-driven MB photo-decomposition should not be dominated by bandgap excitation.

Owing to the wide bandgap, valence band electrons of ZnO cannot be excited by visible light so that MB photodegradationon ZnO is attributed to dye-sensitised photocatalysis. Under visible light illumination MB is excited by light of wavelength shorter than its characteristic absorption wavelength (662 nm) and then injects photoexcited electrons into ZnO conduction band (CB). The electrons injected onto ZnO CB react with soluble oxygen and give rise to active oxygen species which can decompose the excited MB[7, 14]. In contrast, C-doped ZnO may be excited by visible light due to its narrowed bandgap to lift valence electrons onto CB and leave holes on VB. Furthermore, C-doped ZnO should have been shown stronger dye-sensitising effect than ZnO since C-doped ZnO possesses larger S$_{BET}$ and thus sensitising opportunity due to higher MB adsorption amount. It seemed the heavy C-doped ZnO should be more active, whereas the experimental results showed it is less active than ZnO, suggesting heavy C-doping would deteriorate the dye-sensitised photodegradation. It is reasonable to conclude that bandgap excitation of the C-doped ZnO contributes a little to the overall MB photodegradation in comparison to dye-sensitisation under visible-light illumination. The fact is that heavy C-doping and derived Ovac correspondingly would serve as recombination centres in the photoreaction which reduce dye-sensitising effects by trapping the electrons from excited dyes and thus deteriorate photodegradation on C-doped ZnO relative to ZnO.

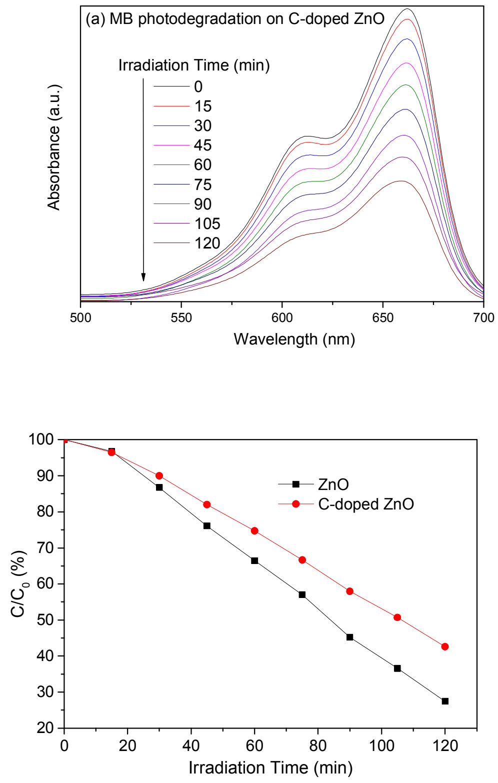

Fig.9 (a) UV-vis spectra on C-doped ZnO and (b) photocatalytic activity on ZnO and C-doped ZnO for Methylene degradation

In general, the enhanced light absorption corresponds to enhanced photoexcitation while the photoexcitons are prone to recombination leading to almost 95% loss of absorbed light energy[4, 5, 24]. The charge recombination centres may be overloaded dopants or structure deficiencies, for instance Ovac. Previous report evidenced there exists optimum C-doping range for promoting visible-light-driven photoreactivity while photocatalytic activity would be lower beyond the suitable C-doping levels[7]. C-doped ZnO containing 2.7 at.% C showed higher activity than that containing 0.41 at.% C-dopant[8]. However, the roles of Ovac were not paid enough attention. We did find the photocatalytic activity may be improved for light-C-doped ZnO prepared through reducing F127 amount (ESI, Fig.S2), while this research focused on the heavy C-doping sample because it is more important to unveil the function of coexistence of C^{4-} and Ovac. Despite the fact that suitable amount of Ovac can extend light absorption into visible light region and improve photocatalytic activity, the photoreactivity will drop dramatically if Ovac concentration is greater than certain amount[15, 23]. In this research, the C-doping level is quite high with almost 4.3 at% carbide-based C^{4-} coexisting with comparable amount of Ovac in the C-doped ZnO. Hence, the low visible-light-driven photocatalytic activity on the C-doped ZnO was tentatively assigned to the synergistic consequences of the overloaded C-dopants and Ovac that favour the recombination of photogenerated charge carriers under irradiation.

4.Conclusion

C-doped ZnOnanoflakes with large surface area were successfully synthesised via a pyrolysis process using Pluronic F127 as polymer-directed agent. The C-doping leads to enhanced UV and visible light absorption yet does not affect the electron (direct) transition characteristic of ZnO. The direct bandgap of the C-doped ZnO is 2.98 eV though its light adsorption tails beyond visible light region because of co-existing oxygen vancancies and C-dopants.

VBM XPS evidenced the C-doping expends VB width of ZnO and lifts its VBM energy as well as draws the CBM down towards Femi level, leading to narrowed bandgap. DFT simulations reveal the origin of visible-light-response of C-doped ZnO is also related to addition bandgap electron states (energy levels) arisen from C-doping and correspondingly created Ovac stemmed from C-doping. Distinguished from O2p and Zn 4s states composing ZnO VBM and CBM, the VBM of C-doped ZnO is dominated with C2p state and its CBM mainly contains Zn 4s along with additional states of Zn 3d and hybridised states of O 2s and O2p of Ovac. Although the C-doped ZnO showed enhanced light absorption, its visible-light-driven activity in MB photodegradation is worse than that ZnO because the C-doping and corresponding Ovac led to significant charge recombination.

Notes and references

[a] *National Nanotechnology Research Center, King Abdulaziz City for Science and Technology, King Abdullah Road, P.O. Box 6086, Riyadh 11442,Saudi Arabia. Tel: 966 (0)11 481 4285; E-mail: aalshammari@kacst.edu.sa*
[b] *Faculty of Engineering and the Environment, University of Southampton, Southampton, SO17 1BJ, UK. Tel: 44(0)2380594893; E-mail: z.jiang@soton.ac.uk*
[c] *School of Environmental Science and Engineering, Shanghai Jiao Tong University, Shanghai,200240, China*
[d] *Department of Chemistry, Inorganic Chemistry Laboratory, University of Oxford, Oxford OX1 3QR, UK*

Acknowledgement: We acknowledge the financial support from the University of Southamtpon (innovation adventure fund), Shell Foundation (Sir John Houghton Fellowship), HEFCE (Zepler institute stimulus fund) and King Abdulaziz City for Sceince and Technology (KACST, project No: 29-280). LC, XC and ZJ thank the support from EU- Ecofuel project (European Commission - FP7, 246772).

† Electronic Supplementary Information (ESI) available: [Fig.S1 PDOS of (a) O and (b) Zn in Wurtzite ZnO crystal; Fig. S2, Methylene Blue Photodegradation over ZnO and C-doped ZnO with different C-doping levels]. See DOI: 10.1039/b000000x/

References

1. A. Kubacka, M. Fernández-García and G. Colón, *Chem. Rev.*, 2011, **112**, 1555-1614.
2. R. E. Galian and J. Perez-Prieto, *Energy & Environ. Sci.*, 2010, **3**, 1488-1498.
3. Y. Tachibana, L. Vayssieres and J. R. Durrant, *Nat Photon*, 2012, **6**, 511-518.
4. A. Ajmal, I. Majeed, R. N. Malik, H. Idriss and M. A. Nadeem, *RSC Adv.*, 2014, **4**, 37003-37026.
5. M. Pelaez, N. T. Nolan, S. C. Pillai, M. K. Seery, P. Falaras, A. G. Kontos, P. S. M. Dunlop, J. W. J. Hamilton, J. A. Byrne, K. O'Shea, M. H. Entezari and D. D. Dionysiou, *Appl. Catal. B*, 2012, **125**, 331-349.
6. M. N. Chong, B. Jin, C. W. K. Chow and C. Saint, *Water Res.*, 2010, **44**, 2997-3027.
7. S. Liu, C. Li, J. Yu and Q. Xiang, *CrystEngComm*, 2011, **13**, 2533-2541.
8. S. Cho, J.-W. Jang, J. S. Lee and K.-H. Lee, *CrystEngComm*, 2010, **12**, 3929-3935.
9. Y.-G. Lin, Y.-K. Hsu, Y.-C. Chen, L.-C. Chen, S.-Y. Chen and K.-H. Chen, *Nanoscale*, 2012, **4**, 6515-6519.
10. S.-M. Lam, J.-C. Sin, A. Z. Abdullah and A. R. Mohamed, *Desalin. Water Treat.*, 2012, **41**, 131-169.
11. F. Wang, L. Liang, L. Shi, M. Liu and J. Sun, *Dalton Trans.*, 2014, **43**, 16441-16449.
12. D. Chen, Z. Wang, T. Ren, H. Ding, W. Yao, R. Zong and Y. Zhu, *J. Phys. Chem. C*, 2014, **118**, 15300-15307.
13. H. Pan, J. Yi, L. Shen, R. Wu, J. Yang, J. Lin, Y. Feng, J. Ding, L. Van and J. Yin, *Phys. Rev. Lett.*, 2007, **99**, 127201.
14. O. Haibo, H. J. Feng, L. Cuiyan, C. Liyun and F. Jie, *Mater. Lett.*, 2013, **111**, 217-220.
15. Z. Jiang, L. Kong, F. S. Alenazey, Y. Qian, L. France, T. Xiao and P. P. Edwards, *Nanoscale*, 2013, **5**, 5396-5402.
16. S. U. M. Khan, M. Al-Shahry and W. B. Ingler, *Science*, 2002, **297**, 2243-2245.
17. K. Yang, Y. Dai, B. Huang and M.-H. Whangbo, *Chemistry of Materials*, 2008, **20**, 6528-6534.
18. K. Yang, Y. Dai, B. Huang and M.-H. Whangbo, *J. Phys. Chem. C*, 2009, **113**, 2624-2629.
19. Wenjie Ren, Zhihui Ai, Falong Jia, Lizhi Zhang, Xiaoxing Fan and Zhigang Zou, *Appl. Catal. B*, 2007, **69** 138–144.
20. D. E. Zhang, M. Y. Wang, J. J. Ma, G. Q. Han, S. A. Li, H. Zhao, B. Y. Zhao and Z. W. Tong, *Funct. Mater. Lett.*, 2014, **07**, 1450026.
21. S. T. Tan, X. W. Sun, Z. G. Yu, P. Wu, G. Q. Lo and D. L. Kwong, *Appl. Phys. Lett.*, 2007, **91**, 072101.
22. D. K. Mishra, J. Mohapatra, M. K. Sharma, R. Chattarjee, S. K. Singh, S. Varma, S. N. Behera, S. K. Nayak and P. Entel, *J. Magnet. Magnet. Mater.*, 2013, **329**, 146-152.
23. J. Wang, Z. Wang, B. Huang, Y. Ma, Y. Liu, X. Qin, X. Zhang and Y. Dai, *ACS Appl. Mater. & Interf.*, 2012, **4**, 4024-4030.
24. S. G. Kumar and K. S. R. K. Rao, *RSC Adv.*, 2015, **5**, 3306-3351.
25. J. P. Perdew, K. Burke and M. Ernzerhof, *Phys. Rev. Lett.*, 1997, **78**, 1396.
26. H. J. Monkhorst and J. D. Pack, *Phys. Rev. B*, 1976, **13**, 5188-5192.
27. A. Bagabas, A. Alshammari, M. Aboud and H. Kosslick, *Nanoscale Res. Lett.*, 2013, **8**, 516.
28. H. Li, Y. Zhang and J. Wang, *J. Amer. Ceram. Soc.*, 2012, **95**, 1241-1246.
29. R. Asahi, T. Morikawa, T. Ohwaki, K. Aoki and Y. Taga, *Science*, 2001, **293**, 269-271.